Int. J. Electrochem. Sci., 15 **(2020)** 515 – 525, doi: 10.20964/2020.01.76

International Journal of
ELECTROCHEMICAL
SCIENCE
www.electrochemsci.org

Gold Sputtering-assisted Conductive Electrospun Nanofibers Mat Decorated with MnO_2 Nanospheres for Flexible, High-performance Supercapacitor Electrodes

Guoxi Luo[1,2], Qiankun Zhang[1], Yunyun Luo[1], Shubei Wang[2], Ping Yang[1], Libo Zhao[1,], Zhuangde Jiang[1]*

[1] State Key Laboratory for Manufacturing Systems Engineering, School of Mechanical Engineering, Xi'an Jiaotong University, Xi'an, Shannxi 710049, China
[2] Xi'an Jiaotong University Suzhou Institude, Suzhou, Jiangsu 215123, China
[*]E-mail: libozhao@mail.xjtu.edu.cn

Received: 18 September 2019 / *Accepted:* 1 November 2019 / *Published:* 30 November 2019

Electrospun nanofibers (ENFs) and mats are regarded as ideal electrode candidates for electrochemical energy storage devices such as supercapacitors (SCs), due to their large specific surface area, three-dimensional (3D) nano architecture, light weight, high porosity, and low cost. However, the technique of electrospinning usually produces polymeric nanofibers, the inferior conductivity of polymers dramatically hinders their direct applications in electrochemistry. In this work, magnetron sputtering is utilized to coat a layer of uniform gold onto the surface of electrospun poly(vinylidene fluoride-trifluoroethylene) (PVDF-TrFE) nanofibers to achieve a highly conductive 3D network, followed with electrodeposition of manganese dioxide (MnO_2) nanospheres as pseudocapacitive materials. The advanced SCs electrode exhibits integrated features of high specific capacitance (ca. 385 F g^{-1} at 1 A g^{-1}), decent rate capability (ca. 50 % retention as the current density is increased from 1 A g^{-1} to 20 A g^{-1}), long cycling life (ca. 94% retention after 2000 charging/discharging cycles), and attractive flexibility. This facile strategy of "sputtering-electrodeposition" shows a great potential to open up a new route for developing various kinds of ENFs-based energy storage devices for flexible electronics.

Keywords: Electrospun nanofibers; Magnetron sputtering; Electrodeposition; Manganese dioxide; Flexible supercapacitor

1. INTRODUCTION

Nowadays, flexible energy storage devices including batteries and supercapacitors have drawn more and more attention attributed to their potential as energy sources for flexible devices and systems, in which that would be difficult to achieve by using the rigid electronics of today. Particularly, flexible SCs possess the advantages of higher power density, longer cyclic lifetime, and

faster charge/discharge rate compared with batteries[1-3], enabling them to be one of the most promising candidates for flexible energy storage devices. In general, the prerequisite to develop the flexible and high-performance SCs electrodes is correct incorporation of electrode substrates with good mechanical flexibility, high specific surface area, and electrochemical stability. Recently, a variety of flexible substrates, such as metallic foams [4, 5], carbon fibers/papers/cloths [6-9], modified polymeric films [10], carbon nanotubes networks [11-13], graphene-based architectures [14-16], and even paper [17, 18], have been successfully utilized as electrode templates to immobilize supercapacitive materials for achievement of flexible SCs.

On the other hand, Electrospinning is probably the most powerful and straightforward method that utilizes electrostatic forces to fabricate continuous polymeric nanofibers [19]. In recent years, various kinds of polymers, including polyacrylonitrile (PAN), polymide (PI), cellulose, poly(vinyl alcohol) (PVA), poly(vinyliden fluride) (PVDF) and so on, have been successfully fabricated into nanofibers through the technique of electrospinning [20]. The electrospun mats made up of nanofibers are regarded as ideal alternatives for flexible SCs electrode templates, because they not only possess large specific surface area as well as willowy 3D self-supported architecture, but also exhibit outstanding flexibility [21]. However, most polymers are non-conductive and inevitably hinder their direct applications as electrochemical electrode skeletons.

To solve this issue, several methods have been developed. One effective strategy is the combination of electrospinning and a post carbonization treatment [22, 23], which produces a conductive web consisted of intermingled carbon nanofibers with mesoporous structures. More importantly, various kinds of pseudocapacitive materials can be in situ synthesized within the fibers during the carbonization process to introduce pseudocapacitor performance [24-26]. Even though the method of carbonization can effectively endow conductivity and electrochemical property for ENFs, the requirements of accurate control over high temperature under an inert atmosphere, along with an extra stabilization procedure to increase thermal stability of the nanofibers, make this process pretty complex and dramatically limit its practical applications. Polymerization of conducting polymers on the surface or within the template of electrospun nanofibers is another methodology to develop ENFs-based SCs [27-29]. This chemical route takes advantages of high electronic conductivity, excellent redox activity, and good flexibility from conducting polymers such as polyaniline (PANI), polypyrrole (PPy), poly(3,4-ethylenedioxythiophene) (PEDOT) to offer the pseudocapacitance behavior. For example, electrospun PAN supported PANI nanofibers were prepared through electrospinning combined with an in situ polymerization process [28]. The core-shell PAN@PANI nanofibers mat gave a specific capacitance of 151 F g^{-1} at a current density of 1 A g^{-1}. In this route, however, the core nanofibers skeletons are still non-conductive, which would restrict the fast transfer of charges and thus decrease the electrochemical kinetics of the as-prepared electrodes. As such, it is still challenging to obtain high specific capacitance and rate capability by use of this methodology.

In this work, a facile strategy of magnetron sputtering combined with electrodeposition is proposed to develop ENFs-based SCs electrodes, as illustrated in Scheme 1. Firstly, a PVDF-TrFE nanofibrous mat is fabricated with electrospinning, followed with a layer of gold coated onto the surface of PVDF-TrFE nanofibers by magnetron sputtering. Then, MnO_2 nanospheres, a kind of classical material in the electrochemical applications, are immobilized onto the PVDF-TrFE@Au

nanofibers through electrochemically deposited method to offer the pseudocapacitive property. With this rational process design, the integrated merits of flexible electrode structure, high specific surface area, and good pseudocapacitance can be obtained to produce flexible, high-performance ENFs-based SCs electrodes.

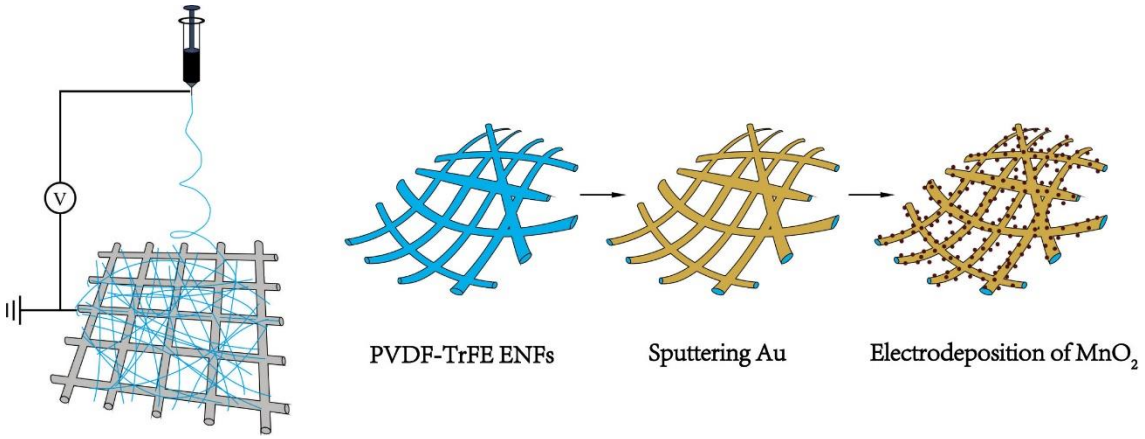

Scheme 1. Schematic illustration of the fabrication process for the advanced electrodes.

2. EXPERIMENTAL SECTION

2.1 Preparation of PVDF-TrFE nanofibers mat

The PVDF-TrFE polymer is selected as ENFs source due to its excellent electrospinnability and homogeneous diameter and morphology of the resulted nanofibers. To prepare the PVDF-TrFE precursor, 1.4 g PVDF-TrFE (Piezotech® FC30, PIEZOTECH ARKEMA) in powder form was firstly dispersed with 4 g of acetone using a magnetic stirrer, and then 6 g of N,N-Dimethylformamide (DMF) was added into the PVDF-TrFE/acetone suspension, finally, the mixture was stirred for at least 3 hours to reach a good homogeneity. The electrospinning was did at the room temperature and 1 atm pressure. The following electrospinning parameters were employed to prepare the PVDF-TrFE nanofibrous mat: applied high voltage of 12.5 kV, the spinneret-to-collector distance of 10 cm, syringe pump rate of 5 μL/min. Then, the electrospun mat was dried in an oven at 70 °C for 12 hours to remove the residual solvent.

2.2 Fabrication of ENFs-based SCs electrodes

Experimentally, a layer of 100 nm gold was firstly coated onto the PVDF-TrFE ENFs by magnetron sputtering equipment (Discovery 635) with a power of 100 W. The sample is denoted as PVDF-TrFE@Au after sputtering. Then, the MnO_2 nanospheres were synthesized through the straightforward electrochemical deposition technique with the three-electrode configuration. The mixture of 20 mM $Mn(NO_3)_2$ and 100 mM $NaNO_3$ (Sigma Aldrich, USA) in DI water was used as aqueous electrolyte. A constant current of 0.5 mA/cm^2 was applied for 10 s, 50 s, and 90 s. The

samples with different MnO_2 electrodeposition time are denoted as PVDF-TrFE@Au@MnO_2-10, PVDF-TrFE@Au@MnO_2-50, PVDF-TrFE@Au@MnO_2-90, Respectively.

2.3. Characterization

The morphology and structure of the as-obtained samples were observed with a field-emission scanning electron microscope (FESEM; SU-8010, HITACHI). Elemental analysis was performed with an energy dispersive X-ray spectrometer (EDS). The crystal structure was characterized by X-ray diffraction (XRD; D8 Advanced, Bruker) using Cu Kα radiation over a 2θ range from 10 to 80°.

2.4 Electrochemical measurements and analysis

The electrochemical measurements of the as-synthesized samples were performed using an electrochemical workstation (Gamry Reference 600+, Gamry Instruments, USA) in 1 M Na_2SO_4 aqueous electrolyte. The as-synthesized samples without any further treatment, platinum foil, and Ag/AgCl electrode were used as working electrode, counter electrode, and reference electrode, respectively. Cyclic voltammetry (CV) tests were enforced in the potential range between 0 and 0.9 V. Galvanostatic charge-discharge (GCD) experiments were carried out with different current densities ranged from 1 A g^{-1} to 20 A g^{-1} in the potential window of 0-0.9 V. Electrochemical impedance spectroscopy (EIS) were tested with the frequency range from 0.01 Hz to 100 kHz using a perturbation amplitude of 5 mV at 0.2 V versus reference electrode. Cycling performance was performed for 2000 charge-discharge cycles at a current density of 10 A g^{-1}.

The calculation of the specific capacitance of the advanced electrode can be obtained from the GCD curves.

$$C = I\Delta t/m\Delta V$$

where the C (F g^{-1}) is the specific capacitance of the as-synthesized electrodes. I (A) is the constant discharging current density. Δt (s) is the discharging time. m (g) is the mass of the active materials on the as-synthesized electrodes. ΔV (V) is the potential window for GCD tests.

3. RESULTS AND DISCUSSION

3.1 Morphology and structure

Fig. 1a shows the typical morphology of the glossy PVDF-TrFE ENFs with the diameter of ca. 250 nm. We can see that the PVDF-TrFE ENFs are randomly oriented but densely packed to form an open microscale structure. This kind of open structure not only provides more surface area, but also promotes electrolyte into the electrode more effectively. The morphology of the PVDF-TrFE@Au sample is displayed in Fig. 1b. The successful coating of 100 nm gold can be clearly distinguished compared with the pristine PVDF-TrFE ENFs, as evident from the increased diameters (ca. 450 nm) and much more coarser surface. This willowy 3D conductive network can supply a conductive path for

electrodeposition of various kinds of pseudocapacitive materials, endowing the capability of ENFs as SCs electrode templetes.

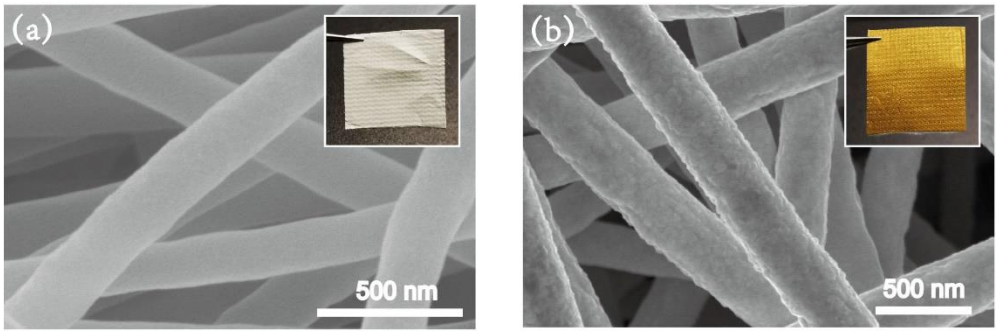

Figure 1. SEM images of (a) PVDF-TrFE ENFs and (b) PVDF-TrFE@Au nanofibers. The insets show optical pictures of the electrospun mat before and after Au sputtering.

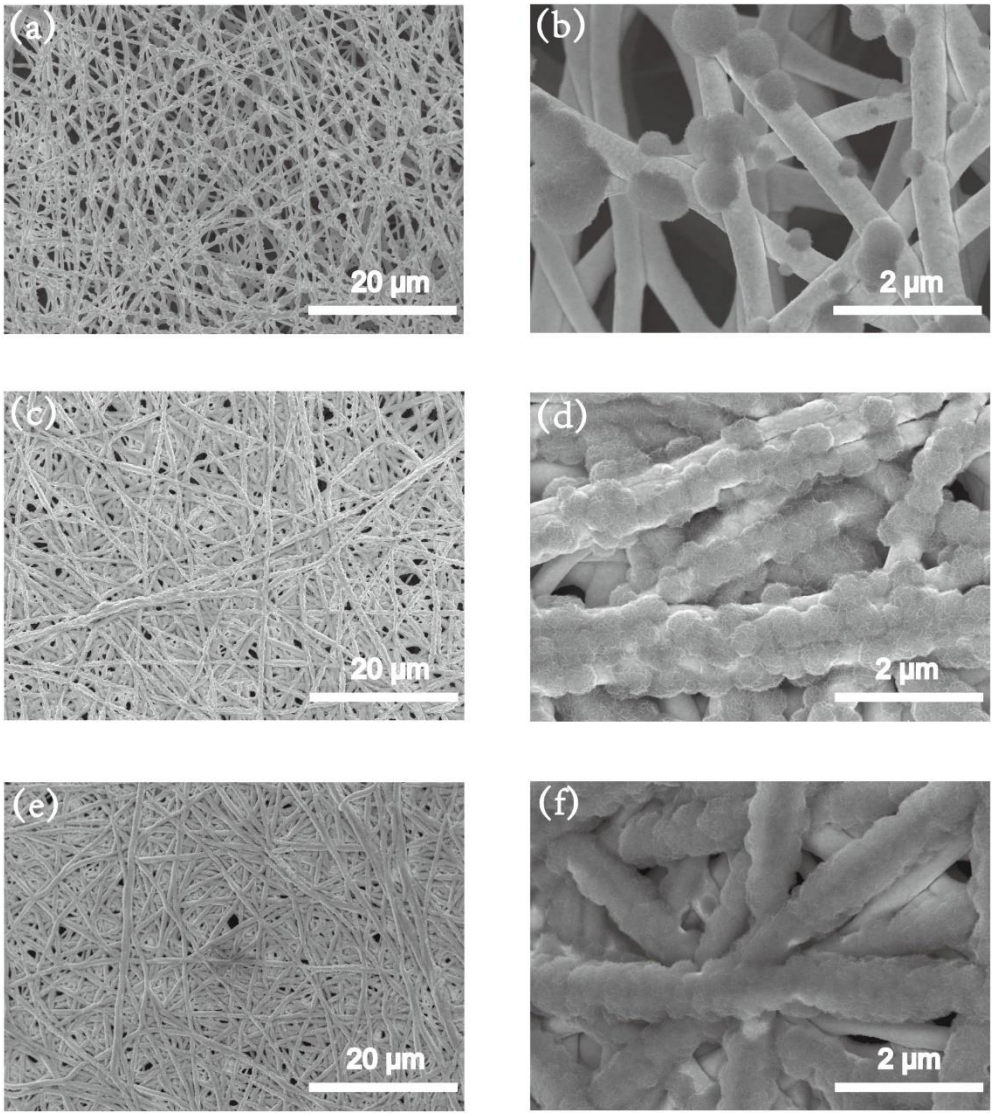

Figure 2. SEM images of (a, b) PVDF-TrFE@Au@MnO_2-10, (c, d) PVDF-TrFE@Au@MnO_2-50, and (e, f) PVDF-TrFE@Au@MnO_2-90.

The electrodeposition time can significantly influences the morphology and quantity of MnO_2 nanospheres, as illustrated in Fig. 2. When the reaction time is 10 s, only a small amount of MnO_2 nanospheres are immobilized onto the PVDF-TrFE ENFs. With elongating the electrodeposition time to 50 s, numerous tiny nanospheres with diameter of ca. 500 nm onto the fibers can be clearly observed. However, as the electrodeposition time is continuously increased to 90 s, more and more MnO_2 nanospheres are formed and interlink each other together to almost cover the entire surface of the PVDF-TrFE ENFs. This would impede the electrolyte infiltration and ion transportation into electrode structure and thus decrease the electrochemical kinetics during the electrochemical reaction [30, 31].

3.2 Materials characterization

The EDS spectrum of PVDF-TrFE@Au@MnO_2-50, as shown in Fig. 3a, offers the clear evidence of the presence of Mn and O elements. Based on the XRD pattern in Fig. 3b, three peaks at 2θ of 23.8°, 37.1°, 66.3° can be observed, these peaks correspond to the (110), (021), and (002) crystallographic planes of MnO_2, respectively [32]. The characterized peaks are not so distinguished due to the nanocrystalline and semicrystalline structure of the electrodeposited materials, suggested by previous references [33, 34]. The XRD results further demonstrate that the MnO_2 has been successfully immobilized onto the PVDF-TrFE ENFs.

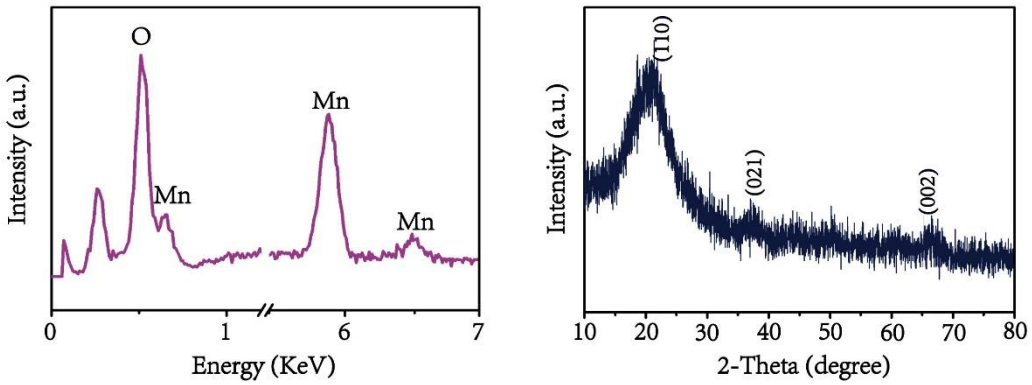

Figure 3. (a) EDS spectrum and (b) XRD patterns of the PVDF-TrFE@Au@MnO_2-50 sample.

3.3 Electrochemical performance

Fig. 4a shows the CV curves of PVDF-TrFE@Au@MnO_2-10, PVDF-TrFE@Au@MnO_2-50, PVDF-TrFE@Au@MnO_2-90 at the scan rate of 60 mV s^{-1}. The CV curve with 10 s electrodeposition time exhibits an approximately rectangular shape (black line) , indicating an excellent reversibility as the quantity of MnO_2 took part in the electrochemical reactions is limited [35]. With extending of electrodeposition up to 50 s, CV curve slightly deviate from rectangular shape (red line). This is mainly due to that more MnO_2 nanospheres are involved into the reactions. However, when the electrodeposition time further increases to 90 s, the CV curve (blue line) exhibits a smaller area as compared to that of 50 s. The reasons can be ascribed to: i) as electrodeposition time rises, more MnO_2

nanospheres are synthesized and interlink each other together to form a continuous structure (Fig. 2f). This morphology would reduce the specific surface area and impede the electrolyte infiltration and ion transportation; ii) the MnO_2 materials are non-conductive in nature, the overly thick layer would limit electron transfer. As such, the overtime electrodeposition would lead to reduction of electrochemical kinetics and decrease the specific capacitance. Based on the GCD curves in Fig. 4b, the gravimetric capacitances at current density of 1 A g^{-1} are 172 F g^{-1}, 385 F g^{-1}, and 258 F g^{-1} for samples of PVDF-TrFE@Au@MnO_2-10, PVDF-TrFE@Au@MnO_2-50, and PVDF-TrFE@Au@MnO_2-90, respectively.

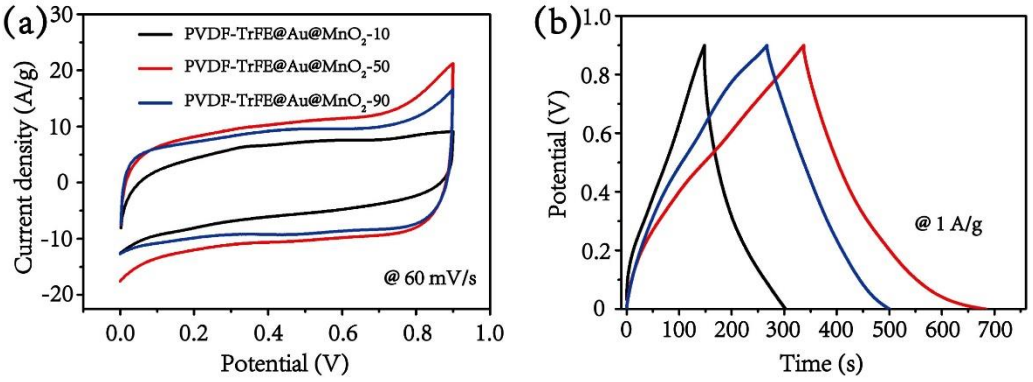

Figure 4. (a) CV and (b) GCD curves for samples of PVDF-TrFE@Au@MnO_2-10, PVDF-TrFE@Au@MnO_2-50, PVDF-TrFE@Au@MnO_2-90

As the optimized electrodeposition time of MnO_2 nanospheres is 50 s in this design, the corresponding sample is utilized for further evaluation of electrochemical performance. Fig .5a shows the CV curves for PVDF-TrFE@Au@MnO_2-50 at different scan rate from 10 mV/s to 100 mV/s. Apparently, the current density is almost proportional to the scan rate, revealing the rapid electronic and ionic transport rate of this advanced electrode [36].

To evaluate the rate capability, the GCD curves of PVDF-TrFE@Au@MnO_2-50 at different current density from 1 A g^{-1} to 20 A g^{-1} in the potential range of 0-0.9 V are measured as shown in Fig 5b, and the gravimetric capacitances at different current densities are calculated and recorded in Fig. 5c. the numerical values are 385, 287, 236, 208, and 191 F g^{-1} when subjected to current densities of 1, 2, 4, 8, and 20 A g^{-1}, respectively. As such, a decent rate capability of ca. 50% is obtained. The rate capability is not so good due to the poor electroconductivity (10^{-5} to 10^{-6} S cm^{-1}) [37] and biggish size (ca. 500 nm in diameter) of the MnO_2 nanospheres. Engineering the MnO_2 nanospheres into smaller size could be an effective method to solve this problem, as this can enable higher utilization ratio of active materials and shorten the diffusion pathway of electrons.

The EIS tests indicate the electrochemical impedance property of PVDF-TrFE@Au@MnO_2-50 in the frequency domain from 0.01 to 100 kHz, as shown in Fig. 5d. The equivalent circuit model [38] is established in the inset. At high frequency, the intersection point on the real axis represents the bulk resistance, R_S, which is the sum of the ohmic resistance of the electrolyte and the internal resistance of the electrode. From the high frequency to midfrequency, a semicircular behavior has been observed, corresponding to the parallel connection of the interfacial charge transfer resistance, R_{CT}, and the double-layer capacitance, C_{DL}. The transition from semicircle to the long tail represents the Warburg

element, W_0, attributed to the ion diffusion in the electrode. At low frequency, the straight line is derived from pseudocapacitance, C_F. Theoretically, R_S and R_{CT} are two main parameters to determine the electrochemical kinetics. According to the Nyquist plot, the R_S and R_{CT} are ca. 5.8 Ω and ca. 8.5 Ω, respectively.

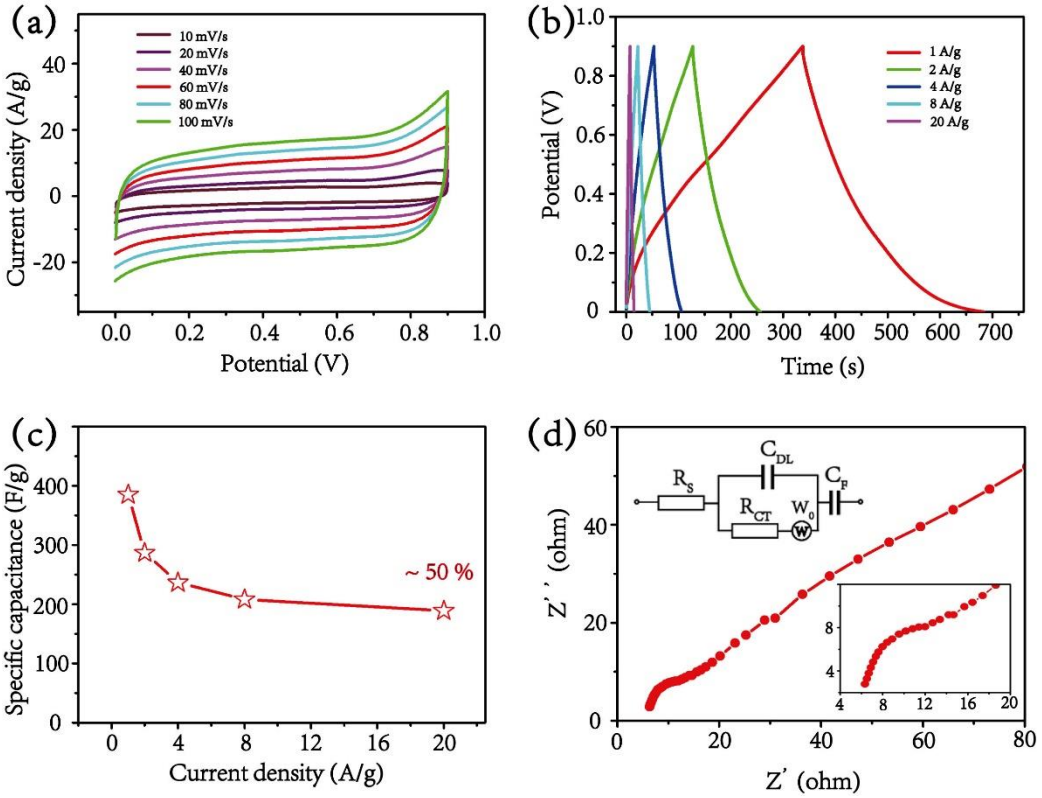

Figure 5. (a) CV and (b) GCD curves for samples of PVDF-TrFE@Au@MnO_2-50 under different scan rates and currrent densities. (c) Rate capability. (d) Nyquist plot of EIS.

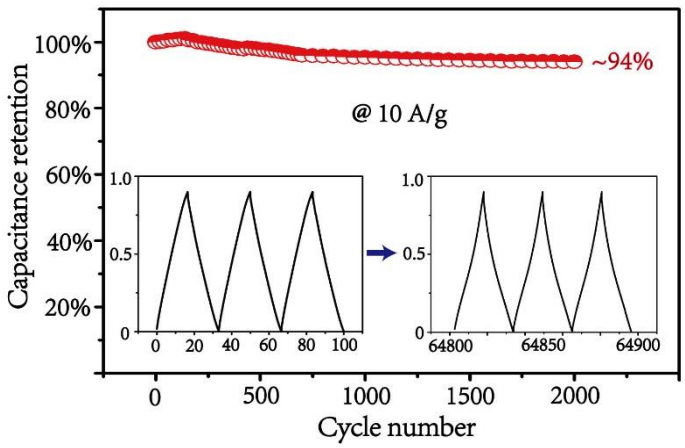

Figure 6. Test of cycling stability at current density of 10 A g^{-1} for 2000 cycles.

The cycling performance is tested by repeated charging/discharging at a constant of current density of 10 A g^{-1} in the potential range from 0 to 0.9 V for 2000 cycles, as illustrated in Fig. 6. The inset exhibits the first and last three cycles of GCD curves, even though shapes of the curves

experience a distortion, about 94 % capacitance retention is still obtained, highlighting the excellent cycling life for this advanced electrodes.

To investigate the mechanical flexibility of the as-prepared electrodes, a sample is bent and twisted by a pair of tweezers, as shown in Fig. 7a and b. After the force was removed, no visible damage was observed. Furthermore, a home-made linear actuator (inset of Fig. 7c) is adopted to introduce repeated mechanical bending upon the sample as shown in Fig. 7c. It can be clearly seen that about 97 % capacitance retention has been obtained after 1000 mechanical cycles. These tests reveal the excellent flexibility and durability of the advanced electrodes.

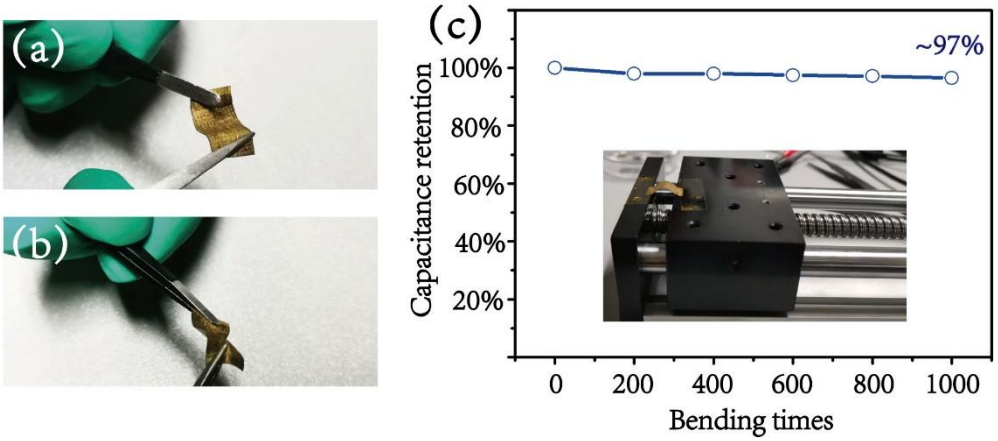

Figure 7. Test of mechanical flexibility.

Table 1. The performance comparison between our work and other literatures for electrodeposited MnO_2-based electrodes used for supercapacitors

Materials	Specific capacitance (F g^{-1})	Mechanical flexibility	References
Electrodeposited MnO_2 on stainless foil	ca. 259 (5 mV/s)	Bad	[39]
Electrodeposited MnO_2 on Cu-decorated Nickel foam	ca. 687 (5 mV/s)	Bad	[40]
Electrodeposited MnO_2 on carbon fiber paper	ca. 363 (0.5 A g^{-1})	Good	[41]
Electrodeposited MnO_2 on graphene-carbon nanofiber	ca. 298 (1 A g^{-1})	Good	[42]
Electrodeposited MnO_2 on rGO paper	ca. 367 (1 A g^{-1})	Good	[43]
PVDF-TrFE@Au@MnO_2-50	ca. 385 (1 A g^{-1})	Excellent	This work

To exhibit the preponderance of our method and electrode, the performance comparison between our electrode and other electrodeposited MnO_2-based electrode composites for supercapacitors is listed in Table 1. It can be clearly seen that our electrode not only exhibits

outstanding specific capacitance, but also possesses excellent flexibility, empowering the advanced electrodes a high potential to be applied as good energy storage devices for wearable electronics.

4. CONCLUSIONS

In conclusion, to overcome the poor electroconductivity of ENFs, a layer of gold is coated onto the surface of PVDF-TrFE nanofibers by magnetron sputtering to fabricate a willowy 3D conductive network, followed with electrodeposition of MnO_2 nanosphere as pseudocapacitive materials. As such, an advanced SCs electrode with integrated merits of high specific surface, 3D nano architecture, light weight, good supercapacitive property, and outstanding flexibility is successfully developed. This novel and facile strategy of "sputtering-electrodeposition" could open up a new route for developing various kinds of ENFs-based energy storage devices for flexible electronics.

ACKNOWLEDGEMENTS
The authors thank Instrument Analysis Center of Xi'an Jiaotong University for the SEM, XRD, and FTIR facilities. This work is supported by the National Natural Science Foundation of China (grant number 51705409), the Natural Science Foundation of JiangSu Province (grant number BK20170415), the Fundamental Research Funds for the Central Universities (grant number xjj2017094), and the Natural Science Basic Research Plan in Shaanxi Province of China (grant number 2018JQ5050).

References

1. K. Jost, D. Stenger, C. R. Perez, J. K. McDonough, K. Lian, Y. Gogotsi, G. Dion, *Energy Enciron. Sci.*, 6 (2013) 2698.
2. P. Yang, W. Mai, *Nano Energy*, 8 (2014) 274.
3. K. Wang, H. Wu, Y. Meng, Z. Wei, *Small*, 10 (2014) 14.
4. M. Li, M. Zhou, Z. Q. Wen, Y. X. Zhang, *J. Energy Eng.*, 11 (2017) 242.
5. D. He, G. Wang, G. Liu, J. Bai, H. Suo, C. Zhao, *J. Alloy Compd.*, 699 (2017) 706.
6. Q. Cheng, J. Tang, J. Ma, H. Zhang, N. Shiya, L. -C. Qin, *J. Phys. Chem. C*, 115 (2011) 23584.
7. L. Huang, D. Chen, Y. Ding, S. Feng, Z. L. Wang, M. Liu, *Nano Lett.*, 13 (2013) 3135.
8. Z. Ye, T. Li, G. Ma, X. Peng, J. Zhao, *J. Power Sources*, 351 (2017) 51.
9. G. Luo, K. S. Teh, Y. Xia, Z. Li, Y. Luo, L, Zhao, Z. Jiang, *J. Alloy Compd.*, 767 (2018) 1126.
10. J. B. In, B. Hsia, J. -H. Yoo, S. Hyun, C. Carraro, R. Maboudian, C. P. Grigoropoulos, *Carbon*, 83 (2015) 144.
11. S. -L. Chou, J. -Z. Wang, S. -Y. Chew, H. -K, Liu, S. -X. Dou, *Electrochem. Commun.*, 10 (2008) 1724.
12. K. Wang, Q. Meng, Y. Zhang, Z. Wei, M. Miao, *Adv. Mater.*, 25 (2013) 1494.
13. Y. G. Zhu, Y. Wang, Y. Shi, J. I. Wong, H. Y. Yang, *Nano Energy*, 3 (2014) 46.
14. Z. Xu, Z. Li, C. M. B. Holt, X. Tan, H. Wang, B. S. Amirkhiz, T. Stephenson, D. Mitlin, *J. Phys. Chem. Lett.*, 3 (2012) 2928.
15. L. Bao, T. Li, S. Chen, C. Peng, L. Li, Q. Xu, Y. Chen, E. Ou, W. Xu, *Small*, 13 (2017) 1602077.
16. Y. Wang, H. Feng, P. Dong, J. Shi, G. Li, L. Zhang, *Int. J. Electrochem. Sci.*, 14 (2019) 3968.
17. S. Hu, R. Rajamani, X. Yu, *Appl. Phys. Lett.*, 100 (2012) 104103.
18. B. Yao, L. Yuan, X. Xiao, J. Zhang, Y. Qi, J. Zhou, J. Zhou, B. Hu, W. Chen, *Nano Energy*, 2 (2013) 1071.
19. C. -L. Zhang, S. -H. Yu, *Chem. Soc. Rev.*, 43 (2014) 4423.

20. J. Xue, T. Wu, Y. Dai, Y. Xia, *Chem. Rev.*, 119 (2019) 5298.
21. X. Lu, C. Wang, F. Favier, N. Pinna, *Adv. Energy Mater.*, 7 (2017) 1601301.
22. C. Kim, K. S. Yang, *Appl. Phys. Lett.*, 33 (2003) 1216.
23. B. Wang, G. Lu, Q. -P. Luo, T. Wang, *J. Nanomater.*, 2016 (2016) 1.
24. Z. Zhou, X. -F. Wu, H. Fong, *Appl. Phys. Lett.*, 100 (2013) 023115.
25. S. Abouali, M. A. Garakani, B. Zhang, Z. -L. Xu, E. K. Heidari, J. -Q. Huang, J. Huang, J. -K. Kim, *ACS Appl. Mater. Interfaces*, 7 (2015) 13503.
26. R. Kumuthini, R. Ramachandran, H. A. Therese, F. Wang, *J. Alloy Compd.*, 705 (2017) 624.
27. A. Laforgue, *J. Power Sources*, 196 (2011) 559.
28. F. Miao, C. Shao, X. Li, N. Lu, K. Wang, X. Zhang, Y. Liu, *Electrochim. Acta*, 176 (2015) 293.
29. W. Ni, J. Cheng, X. Li, G. Gu, L. Huang, Q. Guan, D. Yuan, B. Wang, *RCS Adv.*, 5 (2015) 9221.
30. J. Han, Y. Dou, J. Zhao, M. Wei, D. G. Evans, X. Duan, *Small*, 9 (2013) 98.
31. M. Shao, Z. Li, R. Zhang, F. Ning, M. Wei, D. G. Evans, X. Duan, *Small*, 11 (2015) 3530.
32. S. R. Sivakkumar, J. M. Ko, D. Y. Kim, B. C. Kim, G. G. Wallace, *Electrochim. Acta*, 52 (2007) 7377.
33. G. Luo, K. S. Teh, Y. Xia, Y. Luo, Z. Li, S. Wang, L. Zhao, J. Jiang, *Mater. Lett.*, 236 (2019) 728.
34. L. Hu, W. Chen, X. Xie, N. Liu, Y. Yuan, H. Wu, Y. Yao, M. Pasta, H. N. Alshareef, Y. Cui, *ACS Nano*, 5 (2011) 8904.
35. Z. Zhang, Y. Xiao, Y. Zhang, W. Zhang, *J. Nanosci. Nanotechnol.*, 19 (2019) 5864.
36. C. Yuan, J. Li, L. Hou, X. Zhang, L. Shen, X. W. Lou, *Adv. Func. Mater.*, 22 (2012) 4592.
37. H. Pang, S. Wang, G. Li, Y. Ma, J. Li, X. Li, L, Zhang, J. Zhang, H. Zheng, *J. Mater. Chem. A*, 1 (2013) 5053.
38. B. G. Choi, J. Hong, W. H. Hong, P. T. Hammond, H. Park, *ACS Nano*, 5 (2011) 7205.
39. R. K. Mishra, C. S. Prajapati, R. R. Shahi, A. K. Kushwaha, P. P. Sahay, *Ceram. Int.*, 44 (2018) 5710.
40. S. H. Kazemi, M. A. Kiani, M. Ghaemmaghami, H. Kazemi, *Electrochim. Acta*, 197 (2016) 107.
41. Z. Ye, T. Li, G. Ma, X. Peng, J. Zhao, *J. Power Sources*, 351 (2017) 51.
42. Y. Wu, S. Liu, K. Zhao, Z. He, H. Yuan, K. Lv, G. Jia, *Ionics*, 22 (2016) 1185.
43. H. Li, Y. He, V. Pavlinek, Q. Cheng, P. Saha, C. Li, *J. Mater. Chem. A*, 3 (2015) 17165.